СООБЩЕНИЯ
ОБЪЕДИНЕННОГО
ИНСТИТУТА
ЯДЕРНЫХ
ИССЛЕДОВАНИЙ

Дубна

E9-95-403

V.A.Anosov, M.Billing[1], D.Kaltchev, V.I.Kazacha,
N.Y.Kazarinov, A.K.Krashykh, E.A.Perelstein,
M.Tigner[1], A.T.Vasilenko

ELECTRON-POSITRON HIGH EFFICIENCY CONVERTER[2]

[1]Cornell University, Ithaca, USA
[2]This work was supported by NSF
under contract PHI-9014664 SUB U82-8415

1995

1 Introduction.

The factories such as Phi, Tau- Charm and B-Factories require relatively large positron intensities. Accordingly, new positron converters are required with higher power capability than those now being used in most storage ring injectors. This paper describes the design of a converter which can handle 200 MeV incident beams carrying 6 kW average power. This work is concerned with new possible hardware to produce positrons in the upgraded CESR linac injector by the enhanced power capacity of the converter and improved focusing of the emerging positrons.

Usually the positron producing target is located in a region with increasing magnetic field. The converted positrons move in the increasing magnetic field through a quarter wave transformer (QWT) into the first e^+-linac section. Locating the target in the increasing magnetic field is typical for the existing variants of QWT (DESY [1], LAL [2]). Another example of QWT as implemented at KEK has the target located near the magnetic field maximum [3].

Generally the quarter wave transformer (QWT) is made of short lenses with high magnetic fields (B_i) and a solenoidal magnetic field (B_f) extending over the first e^+-linac sections. In this work it is suggested to design the QWT from two Helmholtz coils (see Fig. 1, position 3). The electron-positron converter (position 2) is placed in the median plane of the QWT, which is located in the middle of the flat top of the magnetic field $B_i(z)$ distribution. In addition it is suggested to increase B_i up to a level of $\sim$ 2.5 T and B_f up to the level of $\sim$ 0.5 T [4]. The conversion efficiency of about 1% can be achieved for an electron beam having r.m.s. diameter $\sigma_r \sim 3$ mm. An additional factor of about 2 may be obtained by decreasing σ_r to 1.5 mm [5]. In [6] it was also suggested to double the positron intensity by reducing electron beam spot on the target, improving the capture solenoid and raising the bombarding energy from 150 MeV up to 200 MeV.

2 Calculations of Positron Production.

All calculations have been made for the following electron beam parameters. The electron beam, impinging on a converter target, has the energy 200 MeV and the following additional constraints [7]:

1. Every beam train, having 2.5 micro second macropulse duration, contains 52 micro bunches of $6 * 10^{10}$ e^-.

2. The beam train repetition frequency f is 60 Hz.

3. The average beam power is about 6 kW.

4. The momentum resolved conversion efficiency for 200 MeV positrons should be equal to 1 %.

5. The r.m.s. electron beam spot diameter on the converter target could be in the range from 1.5 to 3.0 mm.

For these constraints studies of positron capture into the linac sections following the converter have been performed. The momentum resolved conversion efficiency is obtained as the ratio of number of positrons accepted by e^+-linac in the defined energy interval (as required for the booster synchrotron's acceptance) to the number of electrons incident on the tungsten target.

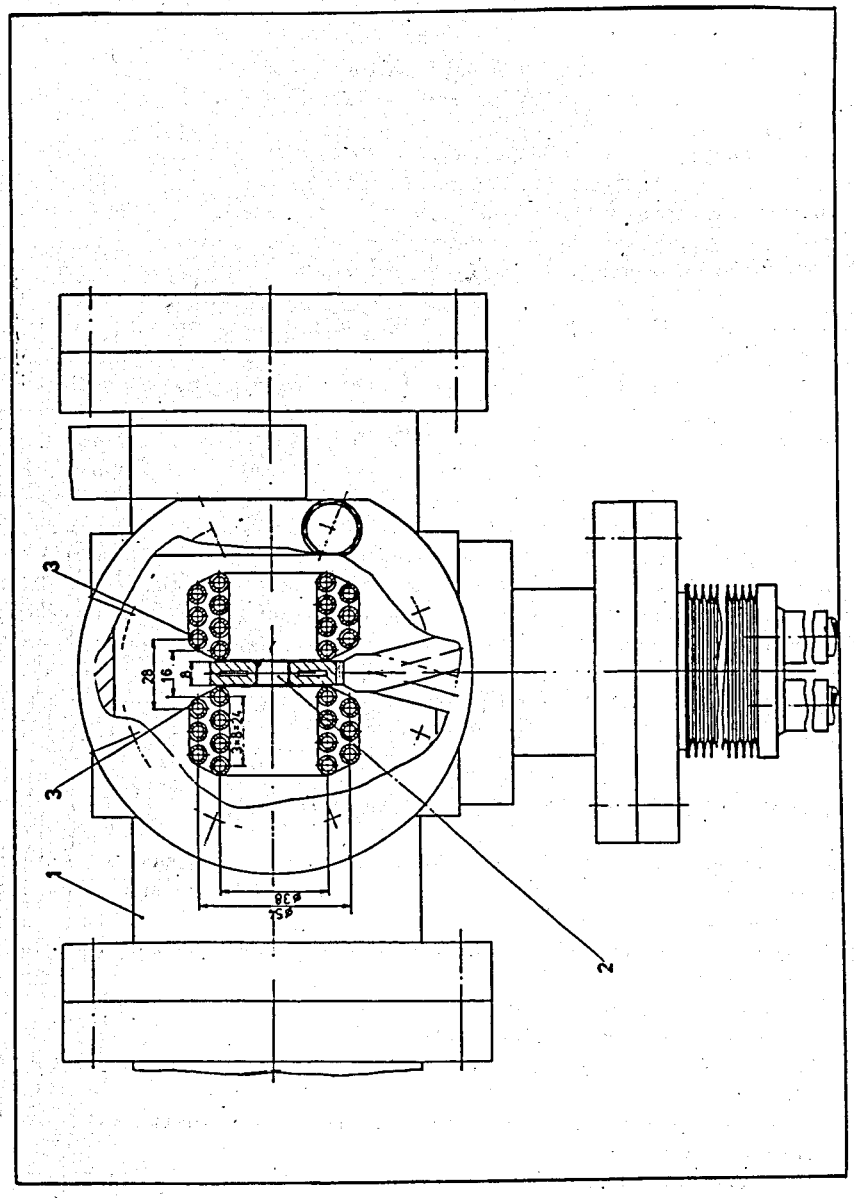
3
3
1
2
28
16
8
3-M5-7H
ø38
ø52

Fig.1

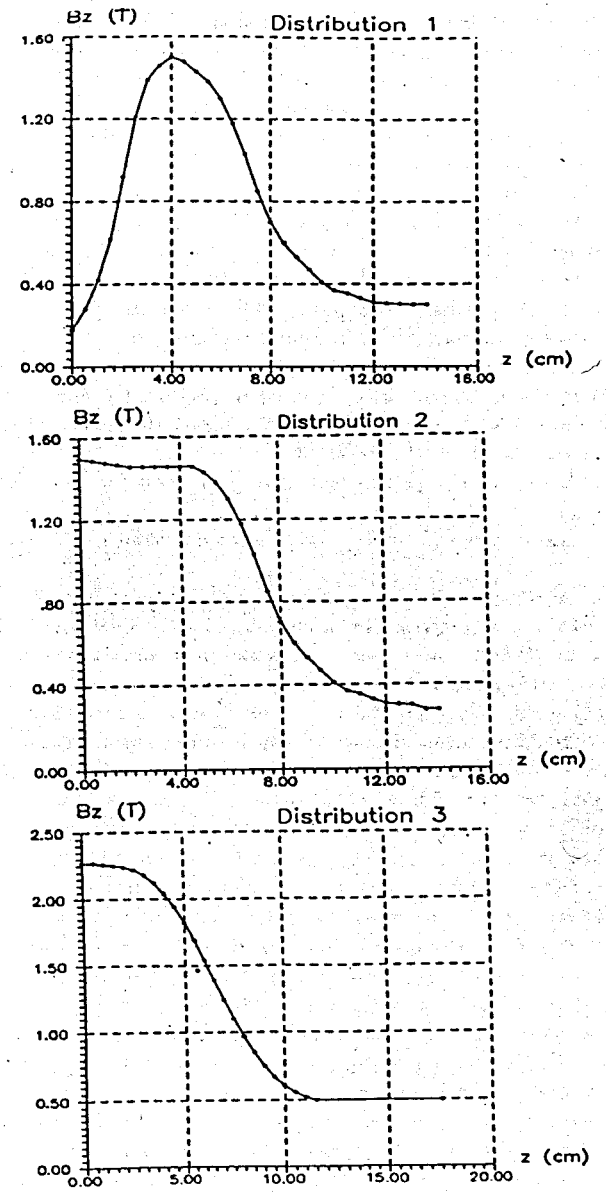
Bz (T)
Distribution 1
1.60
1.20
0.80
0.40
0.00
0.00
4.00
8.00
12.00
16.00
z (cm)
Bz (T)
Distribution 2
1.60
1.20
.80
0.40
0.00
0.00
4.00
8.00
12.00
16.00
z (cm)
Bz (T)
Distribution 3
2.50
2.00
1.50
1.00
0.50
0.00
0.00
5.00
10.00
15.00
20.00
z (cm)

Fig.2

The EGS3 and EGS4 computer codes have been used to simulate positron production inside the target. About 30000 e^-, having a gaussian radial distribution, were generated at the entrance of the target. Simulations have been done for several values of round beam r.m.s. cross-sectional dimensions σ_r and different electron energies. We have neglected the e^- angular distribution because the angular spread of the electron beam is much less than that of the positron beam. To verify the calculations while working with EGS3 code, we also compared the positron radial, angular and energy distributions with those obtained in [8] for a lead target and with results obtained at SLAC [9]. The EGS4 data obtained at SLAC concerned the case: electron energy was E = 200 MeV, electron distribution had the r.m.s. beam diameter σ_r = 0.3 cm, target thickness was 0.7 cm. In a calculation using 10000 e^- we have found a good agreement with [8] and with SLAC data within the statistical errors. The radial and angular positron distributions obtained are also in agreement with the approximate fitting formulae given in [10].

The thickness of the tungsten target is equal to about two radiation length (0.7 cm) and corresponds to the maximum total number of produced positrons. This has been obtained by calculations with several values of the target thickness. The details of these calculations are presented in the APPENDIX I.

The following values of the parameters have been used for the calculations of the present CESR linac:

1. Electron beam energy E_{e^-} = 160 MeV; electron beam r.m.s. dimension σ_r = 3 mm.

2. Conversion target material is tungsten, its thickness is equal to 0.7 cm.

Calculations of the positron conversion efficiency have been carried out in the initial energy interval 5 to 20 MeV. As it has been found with simulations using PARMELA code, this interval corresponds to the positron energy spread of ±5% after acceleration.

We have taken some values for the r.m.s. electron beam size from σ_1 = 3 mm to σ_2 = 0.75 mm. For optimization of positron capture several longitudinal magnetic field distributions were studied. Three of these are shown in Fig. 2. The step size used in the simulation was taken equal to 0.5 cm. Distribution 1 corresponds to the existing QWT field. Distribution 2 may be created by two coils placed symmetrically on the both sides of the target when B_f = 0.3 T and transverse admittance of the first e^+-linac section A_f = 5.3 cm*mrad (see APPENDIX I). Distribution 3 is proposed for the future design. Here B_i = 2.5 T, B_f = 0.5 T, A_f = 8.3 cm*mrad. This magnetic field distribution has been found to give a maximum capture efficiency. In all three cases the target is situated at the point z = 0. The results, as obtained by simulation of the positron capture into the first linac section with the use of the EGS4 code, are given in Table 1.

As it can be seen from this table, one should plan to place the target at the maximum of the QWT magnetic field when designing the converter and to decrease the diameter of the electron beam spot on the target.

Thus we can make the following inferences from the results shown above:

1. The positron conversion efficiency into the first section of the e^+-linac increases up to $\simeq$1% for the proposed magnetic field (distribution 3). In this case the conversion efficiency is about 2.5 times greater than the present operating conditions (distribution 1).

2. An additional factor of about 2 may be obtained by decreasing the electron beam r.m.s. diameter to 1.5 mm. Then the conversion efficiency is obtained equal to (1.6 to 2.0)%.

3. When taking into account the positron longitudinal motion in the first two e^+-linac sections, the conversion efficiency decreases by 15%.

Table 1

r.m.s. beam diameter σ_r mm	Conversion efficiency (distrib. 1)	Conversion efficiency (distrib. 2)	Conversion efficiency (distrib. 3)
0.75	$6.6\ 10^{-3}$	$8.34\ 10^{-3}$	$1.96\ 10^{-2}$
1.5	$5.04\ 10^{-3}$	$6.67\ 10^{-3}$	$1.64\ 10^{-2}$
2.25	$4.5\ 10^{-3}$	$5.23\ 10^{-3}$	$1.26\ 10^{-2}$
3.0	$3.2\ 10^{-3}$	$3.1\ 10^{-3}$	$0.88\ 10^{-2}$

3 Water Cooled Tungsten Converter.

When incident electrons interact with the target there are photons, electrons and positrons produced at the converter output. In order to plan for adequate cooling of the target we need to know the value of the total energy deposited in the target. The following results for the particle energy deposition (see Table 2) have been obtained with EGS3 code. Total incident energy of electrons was equal to 200 MeV.

Table 2

	region #1 before the target vacuum	region #2 tungsten thickness = 7 mm	region #3 after the target vacuum
electrons	0.02%	18.4%	16.9%
photons	0.4%	0.7%	53%
positrons	0.0%	4.6%	5.6%
summary	0.4%	23.7%	75.5%

Thus the total power needed to be removed from the target is about 1.42 kW. The power dissipated in the target has been taken to be 2.0 kW (with ~30% reserve).

The design of the target and its radiator are shown in Fig. 3. The target radiator is made of hard copper of M1 quality. Its parameters are: modulus of elasticity $E_{rad} = 1.26^* 10^6$ kg/cm^2; tensile strength σ_b = 3710 kg/cm^2; yield strength σ_T = 3400 kg/cm^2; thermal conductivity in the temperature span about 100°C λ_{Cu} = 329 kcal/m*hour*degree; coefficient of linear expansion $\beta = 17^*10^{-6}$ 1/degree.

If we assume the temperature of the target radiator is less then 100°C, we can neglect the luminescence of the radiator external surface. All heat released in the target therefore goes into water flowing through the radiator passage.

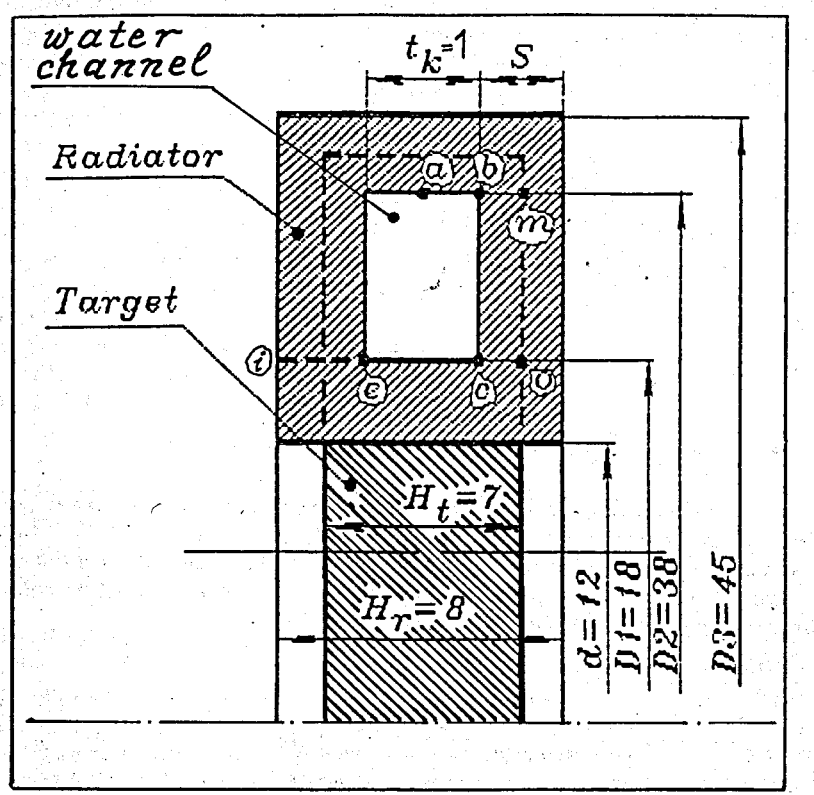

Fig.3

We now consider the steady-state heat flow process cooling the target. The heat flow of Q = 0.48 kcal/sec, corresponding to the entire dissipated power W = 2 kW, is delivered to the target from the electron beam. This heat is transferred through the surface e-a-c from two radiator rings e-i having a width S. Heat is removed into water through surface e-a-c. In the steady-state condition the amount of heat, passing through the ring surface e-i, is equal to the amount, passing through the face surface a-b-c. This is the working assumption for the engineering calculations being carried out below (see APPENDIX II). The target, radiator and water temperature and also temperature stresses have been estimated. They are within admissible limits.

The radiator can be made of a rectangular copper busbar. The target can be soldered to the radiator with lead. Such an approach allows us to relieve the temperature stresses in the radiator body which are due to the large difference in the coefficients of linear expansion of the radiator (Cu) and the target (W) materials.

The radiator outer diameter will not exceed 45 mm. There is a slit in the radiator body that is designed to prevent the formation of a shorted turn. Thus the radiator geometry (shown in Fig. 3) allows us to remove 2 kW of dissipated power from the target when the cooling water flow is equal to 1.8 litr/min with the initial water temperature $t^{o}_{oH_2O}$ = 20°C. One can expect the temperature in the target core to be $\cong$ 500°C and the water temperature rise to be $\cong$ 16°C.

4 Converter Focusing Solenoid

The QWT pulse magnetic field distribution along z-axis has been calculated by summing all turns of the QWT coils. We have used the procedure suggested in [11] for calculating the effects of eddy currents in the vacuum chamber components.

Considering the currents I_o in the coils in free space and then adding the vacuum chamber walls surrounding the coils, we compute the induced eddy currents I_i in the chamber walls by dividing the walls into N small enough axially symmetrical rings. We can write then the following set of equations for the currents induced in these rings:

$$\sum_{i=1}^{N} I_i * M_{ik} = -2\pi * r_k * A_{ok} \qquad (1)$$

where r_k is radius of the ring (having number k); M_{ik} is the mutual inductance of the rings (having numbers i and k); A_{ok} is vector potential due to the coil currents at the chamber wall in the ring having number k. Equation (1) is valid when d $\gg \delta$, where d is the wall thickness and δ is the skin depth, a condition which is true in this case.

The following design of the QWT magnetic field coils shown in Fig. 4 has been chosen accordingly to the results of positron capture simulation presented in section 3. It is proposed that the magnetic field strength be B_z = 2.5 T and be formed by two coils. The mutual coil geometry and the number of the necessary ampere-turns in every coil depend on the following:

1) Parameters for the QWT magnetic field. In our case we have B_z = 2.5 T; the necessary length of this field l = 4.5 cm; f = 60 Hz.

2) Dimensions of the target radiator. As we can see from Fig. 3, the axial radiator dimension H_r is 8 mm. Thus the distance between the coil inner edges must be not less than l_g = 10 mm.

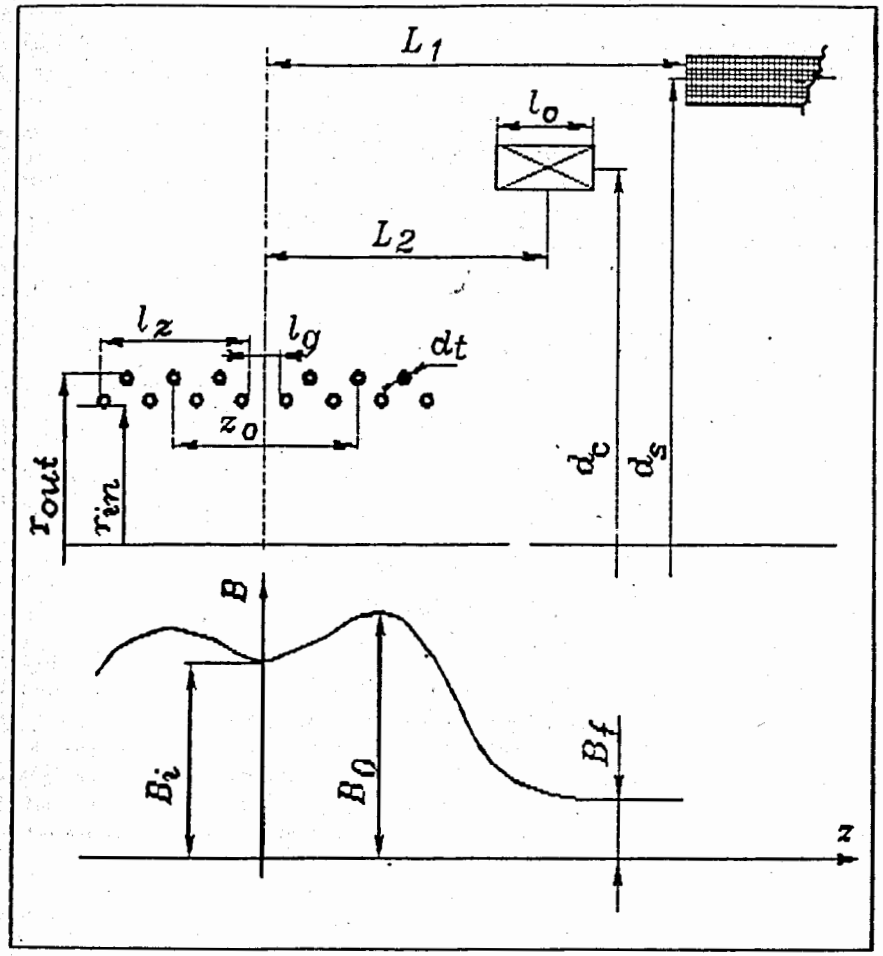

Fig.4

3) The value of the permissible reduction of the QWT magnetic field at the target due to the gap between the two solenoid coils. We assume the reduction of the magnetic field in the target median plane to be not more than 15%.

4) Parameters for the switching device for the magnet pulser. Thyratron mean current must not exceed 10 A.

5) The coil inductance must be as low as possible.

Each coil has the following parameters: length $l_z = 42$ mm; distance between the coil centers $z_c = l_z + l_g = 52$ mm; inner radius $r_{in} = 16$ mm; outer radius $r_{out} = 30$ mm; number of windings w= 7; number of layers $n_l = 2$; amplitude of the current in the coils J = 15 kA. The conductor is a hollow copper pipe with an outer diameter $d_t = 6$ mm and wall thickness $\delta = 1$ mm. The maximum tangential and axial stress in the coil turns is about 120 kg/cm^2 (yield strength for soft copper is equal to 700 kg/cm^2) when the conductor is cooled directly by water.

As it will be shown in the section 5, the half sinewave duration of the magnetic field is rather short (about 15 μs). The dissipated power that should be removed from each coil is about 120 W, which can easily be removed by water with a flow speed of 1 m/sec.

The calculated distribution of B_z on the axis of the system allowing for eddy current effects of the vacuum chamber members is also shown in Fig. 4. The distance L_1 between QWT median plane and front edge of the solenoid ($d_s = 30$ cm) surrounding the first accelerator after the positron target is about 20.5 cm.

In our calculations we have used the existing coil ($l_c = 7.6$ cm; $d_c = 16.5$ cm) as the magnetic field corrector. The distance between the median plane of this coil and the front edge of the solenoid L_2 is about 14 cm. Some little increase of the rate of the QWT magnetic field decay (10%) is attained at the expense of eddy current effects in the vacuum chamber flange.

5 Power Supply for Converter Solenoid

The most natural solution for the design of the pulser and power supply uses the scheme of a capacitor discharged through the coil's inductance by a switch. The choice of the LC-time constant and switch type have been determined as follows:

The characteristics of the pulser are determined by the mutual coil arrangement and their geometrical dimensions which are shown above (Fig. 4). The design of such pulse generators already exists. They continue to operate in the steady-state with pulse currents of about 15 kA into an inductive load. The closest design for such a pulse generator is the modulator which is used as the pulse generator for the SLAC positron production system [12]. In this system 12 thyratrons are required, 8 of them are used for the forward current switch and the remainder are used to protect those eight. The pulse repetition rate of this generator is 120 Hz.

The value of the forward current (I) has also been chosen to be equal to 15 kA in our case. Different pulser designs have been discussed. We have chosen the simplest one for the case when the QWT coils are placed directly in the vacuum chamber. If voltage amplitude (U_o) is limited to the 10 kV level, then the electrical field gradient on the coils will not be more than the typical values for the standard electrical equipment. Thus

metal-ceramic bushing insulators can be used for the feed through the vacuum chamber.

The U_o and I values define main parameters for the pulse modulator for the given geometry of the coils. The selected parameters of the pulser system is given in Table 3. The inductance L (including the mutual inductance) for the free space is given. The inductance calculations have been carried out by method [13]. The accuracy of these calculations is better than 10%.

Table 3

2d	mm	52
$2*r_o$	mm	46
B_i/Bo		0.85
B_o	T	2.5
I*w	kA*turns	105.
L	μH	3.25
U_o	kV	10.
I	kA	15.
r_o	Ohm	0.7
t	μs	15.3
C	μF	7.3
i (aver)	A	8.8

The principal scheme for the pulse generator is shown in Fig. 5. The generator includes thyratron, capacitor C, feedline F, load L and the recuperation circuit Rec. In our case the average current i(aver) is about 9 A and there is rather short half period of the sinusoidal current in the load. We can use a thyratron type of the switch. The thyratron TGI-5000/50 type has the nominal average current 10 A and we would need only one for the generator. Typical parameters of the TGI-5000/50 switch tube are shown below (Table 4). We have chosen this type of the thyratron switch tube for the future design. The generator has two independent channels. Each channel has one thyratron, a capacitance block and a feedline.

The capacitance C can be constructed by the parallel-series connection of the Russian capacitors of FST-4-16 type. These capacitors are designed for work with pulse power systems. Their loss tangent angle is about $55*10^{-4}$. We will not need a fan for the capacitors. The total number of the capacitors is 12 with a total weight of 336 kg.

The feedline may be built from lengths of flexible coaxial cables (25 cables in parallel connection). For example, we could use PK-50-11 coaxial cable having 50 Ohm impedance with OD = 11 mm.

Varying the magnetic field level is possible by changing the voltage on the storage capacitors or by changing the delay of the trigger relative to the beam on the target. A Rogovsky coil may be used to control the pulse current. A preliminary design for the generator is shown in Fig. 6.

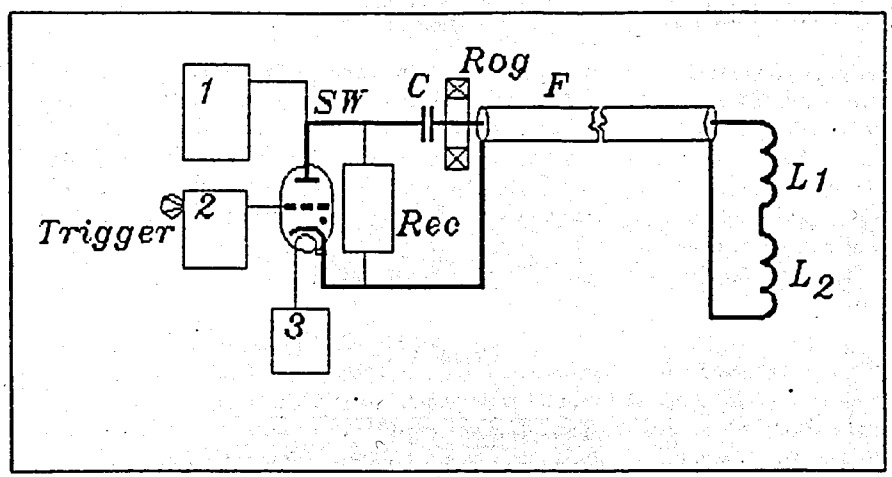

Fig.5

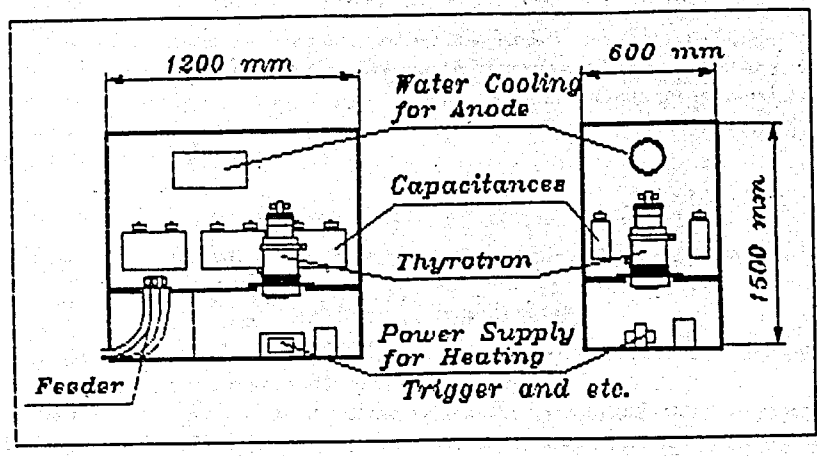

Fig.6

6 Conclusion

This work provides the engineering calculations for all converter systems. It is shown that a conversion efficiency of about 1% can be obtained for the electron beam with energy 160 to 200 MeV and average beam power of about 6 kW by means of the present converter design. This increased conversion efficiency was obtained by increasing the magnetic field B_i level up to $\sim$ 2.5 T at the target and the solenoidal magnetic field B_f level up to $\sim$ 0.5 T. The present converter design unlike other designs has the target located on the flat top of $B_i(z)$ field distribution.

This converter design is compatible with use in the existing CESR linear injector for testing.

Table 4

Anode voltage	kV	50
Pulse current	kA	5
Pulse duration	μs	16
Repetition rate	Hz	125
Average current	A	10
Heating current	A	178-202
Heating voltage	V	6.0-6.6
Trigger grid voltage	kV	+(1.2-2.5)
Duration of the trigger grid voltage	μs	3.0

APPENDIX I

Positron Transportation through QWT and Capture Conditions.

Data for every positron are stored according to the standard EGS output table and are used as input into the QWT-simulation program. At the exit of the target where the magnetic field level is B_i every positron is characterized by:

E – total positron energy;

x_o and y_o – initial coordinates;

$x_o^{'}$ and $y_o^{'}$ – initial angles with respect to z-axis.

These data are used to calculate the particle movement in the magnetic fields by stepping spatially along the accelerator. An attempt to calculate the positron conversion efficiency into the first e^+-linac section immersed in B_f with the help of PARMELA code has been unsuccessful. Therefore another method was devised to compute the positron transport for an arbitrary magnetic field distribution and it is described as follows.

The magnetic field distribution is approximated by a stepwise constant B-field function with step length dz along the longitudinal axis. In every interval of constant B the coordinates $x_{1,2}$ and the angles $x_{1,2}^{'}$ at the beginning and at the end of the interval are computed by the linear transformation (valid in a coordinate frame which rotates with a Larmor angular frequency).

$$\begin{pmatrix} x_2 \\ x_2^{'} \end{pmatrix} = \begin{pmatrix} cos(k_1 * dz) & 1/k_1 * sin(k_1 * dz) \\ -k_1 * sin(k_1 * dz) & cos(k_1 * dz) \end{pmatrix} * \begin{pmatrix} x_1 \\ x_1^{'} \end{pmatrix}, \qquad (2)$$

where $k_1 = eB_i/2cp_{z1}$ is the Larmor wave number of a particle having longitudinal momentum cp_{z1} in magnetic field B_i and dz is the length of a constant magnetic field interval. The same transformation is used in $y, y^{'}$ - plane. We use the energy conservation to find the transformation of the positron longitudinal momentum p_z at the transition from magnetic field strength B_1 to B_2:

$$cp_{z2} = [1 + 2(k_1 - k_2)(x_2^{'}y_2 - y_2^{'}x_2) + (k_1^2 - k_2^2)(x_2^2 + y_2^2)]^{1/2} * cp_{z1} \qquad (3)$$

At the magnetic field transition the angles $x^{'}$ are transformed according to the rule:

$$cp_z x^{'} = const; \qquad cp_z y^{'} = const \qquad (4)$$

Using equations (2 through 4) recursively we can find the transverse coordinates and momentum for any arbitrary magnetic field distribution.

A particle will be captured into the admittance of the accelerating section immersed in a solenoidal magnetic field B_f if its coordinates and angles satisfy the following conditions:

$$k_f x^2 + 1/k_f * x^{'2} \leq A_f \qquad (5)$$

(and the same for $y, y^{'}$ plane), where $k_f = eB/2cp_{zf}$ and $A_f = k_f a^2$ is the transverse admittance of the first e^+-linac section.

APPENDIX II

Temperature Heat Conditions.

The target is made of tungsten having diameter d = 12 mm and length H_t = 7 mm. The thermal conductivity of tungsten is λ_w = 124 kcal/m*hour*degree for an average temperature t^o_{tar} = 300°C. The contact area of cooling water with the radiator F has to be greater than the area defined from the condition [14]

$$F_{cr} = Q/q_{cr}, \tag{6}$$

where q_{cr} = 347.2 kcal/sec*m^2 is the critical heat flow below the boiling point. We obtain from (6) F_{cr} = 1.38*10^{-3} m^2. In our case F $\simeq$ 2.0*10^{-3} m^2. The area of the surface a-b-c is F' $\simeq$ 0.94*10^{-3} m^2.

The average temperature difference Δt^o_{ww} between the radiator walls and water is equal to

$$\Delta t^o_{ww} = Q/\alpha F, \tag{7}$$

where α is heat transfer coefficient into water calculated for a flow speed of v = 3.0 m/sec at the average water temperature $t^o_{H_2Oav}$ = 28°C. The following parameters for water correspond to this temperature: water density γ = 996.2 kg/m^3; water heat capacity C_p = 0.998 kcal/kg*degree; Prandtl number Pr_{H_2O} = 5.74; water viscosity ν = 0.906*$10^{-6}$$m^2$/sec; water thermal diffusivity λ_{H_2O} = 52.3*10^{-2} kcal/m*hour*degree [15].

We must then find Re (Reynolds number) and Nu (Nusselt number) to determine the value for the parameter α:

$$Re = v * d_e/\nu \ ; \qquad d_e = 4 * F_{kn}/P \tag{8}$$

where P is perimeter of the passage cross section. This gives us d_e = 1.8 mm, Re = 6390, Nu = 0.023*$Pr^{0.4}_{H_2O}$*$Re^{0.8}$ = 51.3, $\alpha = Nu*\lambda_{H_2O}/d_e$ = 4.14 kcal/m^2*sec*degree and $\Delta t^o_{ww} \simeq$ 58°C. This temperature rise is permissible.

From the following equation we can determine what the temperature rise $\Delta t^o_{H_2O}$ will be when the power load Q = 0.48 kcal/sec:

$$\Delta t^o_{H_2O} = Q/v * F_{kn} * \gamma * C_p = 16.1°C, \tag{9}$$

where F_{kn} = 10 mm^2 is the cross section of the radiator passage and v = 3 m/sec. Thus the water flow will be V_{H_2O} = v*F_{kn}*60 = 1.8 litr/min.

Heat Q_1 goes from the target into water on the area e-c (see Fig. 3) with the temperature rise Δt^o_{radl}. Let us assume that heat Q_2 goes into water at the area e-a-c from some median surface (containing the points m-o) with the same temperature rise Δt^o_{radl}. We now may obtain this temperature rise from the heat Q = $Q_1 + Q_2$. The temperature rise on the ring having the width t_k is

$$\Delta t^o_{radl} = Q_1/(2\pi * t_k * \lambda_{Cu}) * \ln(D_1/d) \tag{10}$$

and the temperature rise on the area e-a-c is

$$\Delta t^o_{radl} = 0.5 * S * Q_2/(2 * F' * \lambda_{Cu}), \tag{11}$$

where S is shown in Fig.3 (S = 3.5*10^{-3} m). We have from (10 and 11):

$$Q_1/(2\pi * t_k) * \ln(D_1/d) = S * Q_2 * 0.5/(2 * F') \tag{12}$$

Thus we obtain Q_1 = 0.006 kcal/sec, Q_2 = 0.474 kcal/sec and $\Delta t^o_{radl} \cong$ 4.8°C.

The radiator temperature rise will be equal to the sum of two temperature rises: the first one is on the target-ring surface e-i and the second one is on the middle surface m-o surrounding the cooling water channel. We obtain

$$\Delta t^o_{rad} = Q_2/(2\pi * (H_t - t_k) * \lambda_{Cu}) * \ln(D_1/d) + \Delta t^o_{radl} \cong 60.6°C \tag{13}$$

The temperature gradient of the radiator is specified by the temperature difference

$$\Delta t^o_{rad} - \Delta t^o_{ww} \cong 12.2°C \tag{14}$$

In the steady-state conditions we can expect stress in the radiator to be of the order of

$$\sigma^t_{rad} = \beta * (\Delta t^o_{rad} - \Delta t^o_{ww}) * E_{rad} \cong 229 \ kg/cm^2 \tag{15}$$

For this case the yield strength of copper is 3700 kg/cm^2.

The target temperature will be equal to

$$t^o_{tar} = \Delta t^o_{rad} + \Delta t^o_{ww} + \Delta t^o_{H_2O} + t^o_{oH_2O}, \tag{16}$$

where t^o_{oH2O} is the initial temperature of cooling water. Taking $t^o_{oH_2O} = 20^oC$, we have $t^o_{tar} \cong 155°C$.

We assume that the electron beam cross-section dimension is 3 mm. The hot spot in the target will have the same dimension and its temperature will be

$$t_{cor} = Q * \ln(d/d_{core})/(2\pi * H_t * \lambda_w) + t^o_{tar} \cong 530°C \tag{17}$$

References

[1] G. Stange, IEEE Tranc. Nucl. Science, NS-26, $N°3$, 1979, p.4146.

[2] R. Belbeoh et al., Rapport d'etudes sur le project des linacs injecteurs de LEP (LIL), LAL PI 82-01/T, LAL Orsay, 1982.

[3] A. Enomoto et al., Nucl. Instr. and Methods in Phys. Research, A281, 1989, p.1.

[4] E. Perelstein et al., Electron/Positron High Power Converter and Pulsed Lens, PAC-93 Conference Guide, Washington (USA), 1993, p.97.

[5] M. Billing and N. Kazarinov, Preprint CBN 93-5, The Possibility of Increasing the Positron Production for CESR Injection, Cornell University, Ithaca (USA), 1993.

[6] S.X. Fang, The BEPC Upgrade, Proceedings of Third Workshop on the Tau-Charm Factory, Marbela (Spain), 1993,p.5.

[7] K. Berkelman et al., CESR-B Conceptual Design for a B Factory Based on CESR, CLNS 91-1050, Cornell University, Ithaca, NY 14853.

[8] R. Chehab, Positron sources, LAL-RT 89-02, 1989.

[9] Tan Cheng Yang, Optimization of Positron Production at Wilson Laboratory, Cornell University, Ithaca, 1992; R.Nelson (private communication).

[10] H. Braun et al., A possible design for the NLC e^+ source, SLAC-PUB-5746, 1992.

[11] Yu.S. Derendyaev et al., JINR Communication, P9-9140, Dubna, 1975.

[12] J. de Lamar et al. IEEE Particle Accelerator Conference, San Francisco, California, 1991, p.3138.

[13] P.L. Kalantarov, L.A. Zeitlin, Calculation of Inductances, Leningrad, 1986.

[14] S.S. Kutateladze et al., Handbook on heat transfer, Moscow-Leningrad, 1959.

[15] V.S. Chirkin, Thermal physical properties of materials, Moscow, 1959.

Received by Publishing Department
on September 18, 1995.